Complexity Project
Investigating the statistical behaviour of the Oslo Model

CID: 01701209

17th February 2022

Abstract: In this project, we implemented a computer simulation for the Oslo model using Python. A wide range of system sizes from 4 to 1024 was modelled. To minimise the effect of statistical fluctuation, a million iterations after a system has reached the steady state and 20 realisations were performed for each system size. Overall, this leads to accurate results and negligible uncertainties. During our investigation, we studied the self-organised criticality and the scale-free behaviour of the Oslo model for $L \gg 1$. Most notably, we successfully collapsed our data onto a scaling function in multiple instances, indicating a 'blueprint' exists and governs the statistical behaviour in all systems sizes.

Word count: 2483 (discounting the front page)

1 Introduction

The Oslo model was used to model experiments on a continuously driven rice pile which displays self-organised criticality. When a local slope of the pile exceeds its threshold slope, the system responds with an avalanche. This spontaneously drives the system into a non-equilibrium steady state. Complexity emerges as the system grows and is only governed by the fundamental rules, which the Oslo model accounts for by only allowing two threshold slope values. Interesting, the behaviour of the system can be used to study many seismic systems in the real world, such as stock market crashes.

2 Task 1: Implementing the Oslo Model

2.1 Algorithm

The algorithm for the Oslo model is given in the Complexity Project Notes [1], hence is not included in this report.

2.2 Code optimisation

To maximise efficiency, we operated the code in a no-python compilation mode using an external package called Numba. The technique reduced the amount of time to run a simulation by 20 folds. This allowed us to run more iterations, more realisations and larger system sizes for better statistics to perform data analysis on.

2.3 Validation tests

2.3.1 Test 1: Comparing to theoretical values

To validate the programme, we first compared some of our measurements with their theoretical values. First, the average height at site $i = 1$ after the system has reached the steady state was measured to be 26.51 for $L = 16$ and 53.87 for $L = 32$ with a hundred thousand grains added, agreeing well with the values given in the Project Notes [1]. Second, the number of recurrent configurations in $L = 4$ was also determined. The test involves continuously driving the system until the number of recurrent configurations matches its textbook value, 34 [2]. An extra million iterations were conducted to ensure there is no other configuration.

2.3.2 Test 2: Comparing to the BTW model

Another approach is to compare the behaviour of the Oslo model with the one-dimensional Bak-Tang Wiesenfeld (BTW) model. By definition, the BTW model only allows threshold slopes z_i^{th} of 1. This results in more straightforward properties, for example, it is only possible to have one recurrent configuration independent of system sizes. Considering the case where the model is now boundary-driven, the avalanche size s once the system has entered the steady state must always equal the system size because any new grain will immediately topple down the slope and exit the pile. In contrast, since z_i^{th} are allowed to vary in the Oslo model, s is not a fixed quantity. Figure 1 contains our results for $L = 16$.

2.3.3 Test 3: Measuring the probability distribution of threshold slopes

In addition, we investigated the probability distribution of threshold slopes in the stable configurations for the Oslo model. Although the two threshold slopes are chosen with equal prob-

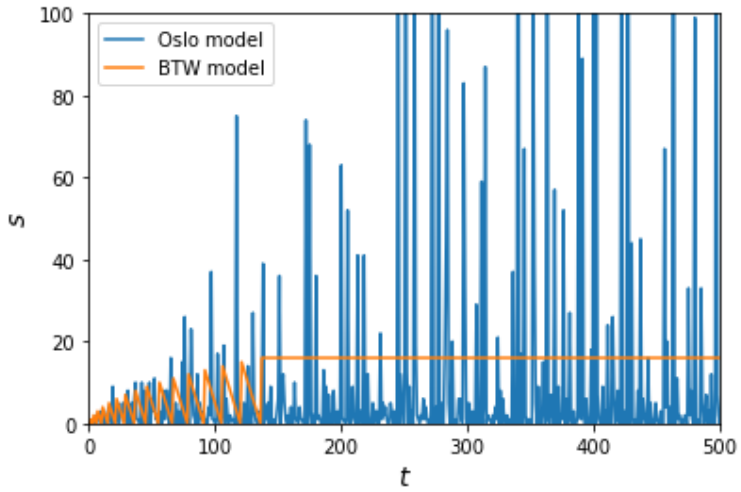

Figure 1: A plot that shows how the avalanche size s varies with time t for the Oslo model (blue) and the BTW model (orange) for $L = 16$. Same as our expectation, the avalanche size the system has reached the steady state remains constant in the BTW model and is identical to the system size. On the other hand, the avalanche size continues to fluctuate in the Oslo model.

abilities, we expect a bias towards $z_i^{th} = 2$. This is because $z_i^{th} = 2$ is the less stable threshold of the two, meaning sites with this threshold slope are reset more frequently than those with $z_i^{th} = 1$. Indeed, the average probability for a site to be in $z_i^{th} = 2$ before reaching the steady state was measured to be 0.65 for $L = 16$.

3 Task 2: Investigating the height of the pile $h(L;t)$

3.1 Task 2a: Measuring the height of the pile $h(L;t)$ over time t

We measured the height of the pile $h(L;t)$, defined as the number of grains at site $i = 1$, for a range of system sizes including $L = 4$, 8, 16, 32, 64, 128, 256, 512 and 1024. To ensure sufficient data for calculating averages for the later tasks, an additional one million iterations were run for each system after one has entered the steady state.

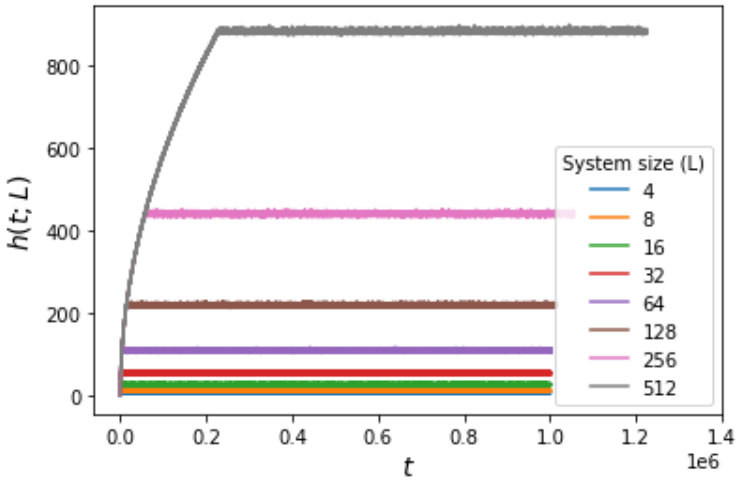

Figure 2: A plot that shows how the height of the pile $h(L;t)$ varies with time t for a range of system sizes. Note only system sizes up to $L = 512$ were plotted for clarity.

In Figure 2, the transient and recurrent configurations correspond to the curved region and flat region of each system size respectively. By definition, the transient configurations happen once only whereas the recurrent configurations can repeat indefinitely. Physically the transient configurations represent the state when the pile is building up but has yet to overflow. For the recurrent configurations, they follow after the system has reached the steady state where the number of grains added equals the number of grains leaving on average, hence the height oscillates around a mean value.

3.2 Task 2b: Measuring the cross-over time $t_c(L)$

The cross-over time $t_c(L)$ was measured as the total number of grains added to the system before causing an overflow for the first time. To minimise the effect of statistical fluctuations, we computed an average of the cross-over time $\langle t_c(L) \rangle$ over 20 realisations for all system sizes. The results were recorded in Figure 3, where we found that $\langle t_c(L) \rangle \propto L^2$ for $L \gg 1$. A power law,

$$f(L) = a \cdot L^k \tag{1}$$

was fitted nicely to the data, where a was determined to be 0.84 ± 0.01 and k is 2.00 ± 0.00 (with all fits uncertainties were estimated using the covariance matrix).

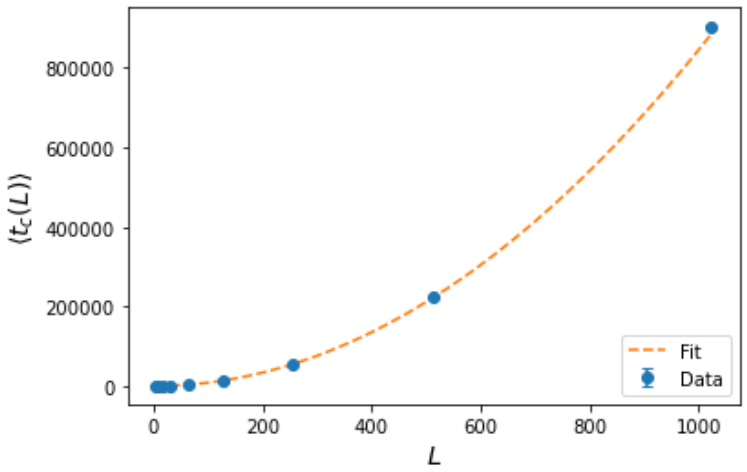

Figure 3: A plot that shows how the average cross-over time $\langle t_c(L) \rangle$ varies with system size L. A power law was fitted to the data, where the exact relationship was found to be $\langle t_c(L) \rangle = (0.84 \pm 0.01) \cdot L^{(2.00 \pm 0.00)}$. Note the uncertainties of the data points were estimated from their standard error of the mean.

3.3 Task 2c: Explaining the scaling behaviour of the average pile height $\langle h(L;t) \rangle$ and average cross-over time $\langle t_c(L) \rangle$

The height of the pile and its cross-over time are intrinsically related to every local slope in the system:

$$h(t;L) = \sum_{i=1}^{L} z_i(t), \tag{2}$$

$$t_c(L) = \sum_{i=1}^{L} z_i \cdot i. \tag{3}$$

3.3.1 Average pile height $\langle h(L;t) \rangle$

The slope at any site can only be 0, 1 or 2. Considering the extreme cases in a given system where all its slopes $= 0$ and all its slopes $= 2$, according to Equation 2, $h(L;t)$ always maps

onto the lines $y = 0$ and $y = 2 \cdot L$. This means that in all circumstances, $h(L;t)$ must be found inside the area bounded by the two lines. Only a linear relationship fits this criterion for $L \gg 1$, hence it follows that $\langle h(L;t) \rangle \propto L$.

3.3.2 Average cross-over time $\langle t_c(L) \rangle$

On the other hand, Equation 3 is essentially the same as calculating the area of the whole pile. Although not entirely, the shape of the pile can be well approximated to a right-angled triangle where its area is equal to one-half of the pile height times the system size or

$$area = b \cdot L^2, \tag{4}$$

b is a proportionality constant. This follows that $\langle t_c(L) \rangle \propto L^2$.

3.4 Task 2d: Producing a data collapse for the processed height $\widetilde{h}(t;L)$

3.4.1 Method

To smooth out the data, we re-computed the height $\widetilde{h}_i(t;L)$ at each site by averaging over 20 realisations for all system sizes. From the scaling behaviour of $\langle h(L;t) \rangle$ and $\langle t_c(L) \rangle$, we know that $h(L;t)$ is a different function for every system size. To remove the dependence of the system on L, we shall re-scale $\widetilde{h}(t;L)$ to $\widetilde{h}(t;L)/L$ and t to t/L^2, introducing the scaling function:

$$F(x) = F\left(\frac{t}{L^2}\right) = \frac{\widetilde{h}(t;L)}{L}, \tag{5}$$

equivalently in its scaling form (as requested by task 2d):

$$\widetilde{h}(t;L) = L \cdot F\left(\frac{t}{L^2}\right). \tag{6}$$

The fact that Equation 5 is only a function of one variable $x = t/L^2$ allows us to produce a data collapse (see Figure 4a) by plotting the re-scaled quantities.

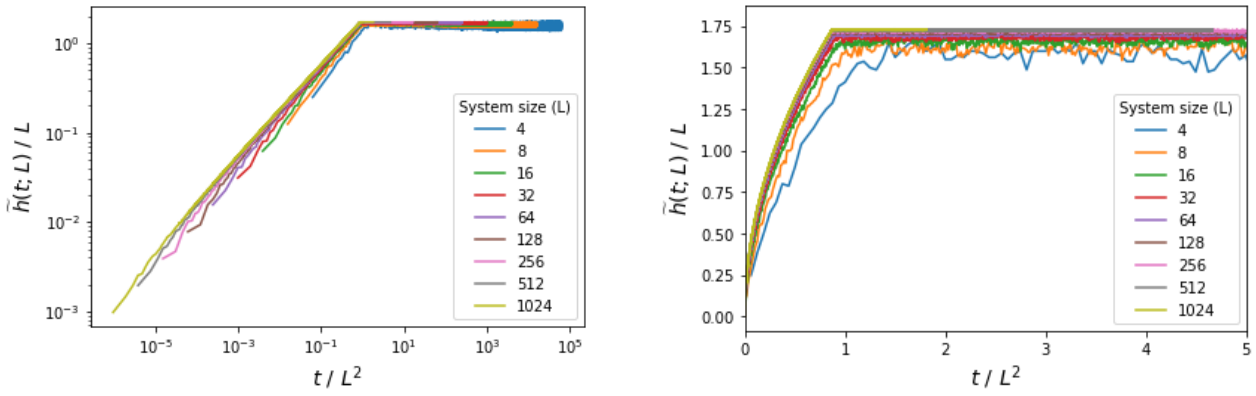

(a) (b)

Figure 4: (a) A broad view of the data collapse on a log-log plot. (b) An enlarged view of the data collapse.

3.4.2 The Behaviour of the scaling function $F(x)$ for different arguments

From Figure 4a, it is evident that $F(x)$ follows a power law for small arguments and is constant for large arguments:

$$F(x) = \begin{cases} a \cdot x^k & x \ll 1 \\ c & x \gg 1 \end{cases}$$

This must be the case because the Oslo model exhibits self-organised criticality, meaning the pile spontaneously organises itself towards a steady state where the average of the net flux is zero. At the critical point, the system transitions from the transient configurations to recurrent configurations, indicated by the sharp discontinuity in Figure 4.

3.4.3 Measuring the scaling relationship of the processed height $\widetilde{h}_i(t; L)$

A close-up look of the data collapse (see Figure 4b) indicates that as the system size increases, the quality of the data collapse onto the $F(x)$ also increases. Therefore, for any measurement with the data collapse, we shall continue with the largest system size. To measure the behaviour of $\widetilde{h}(t; L)$ during the transient, the first 500 data points of $L = 1024$ were fitted with a power law (see Figure 5), where a was measured to be 1.40 ± 0.01 and k is 0.54 ± 0.00. In addition, other features were measured using also $L = 1024$, for example, the discontinuity was found at 0.86 ± 0.00 and $c = 1.73 \pm 0.00$ (uncertainties are negligible because of the large sample size).

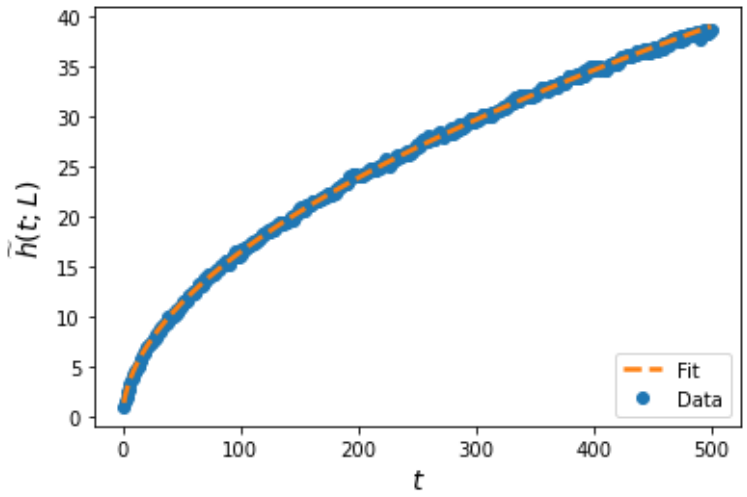

Figure 5: A plot that shows the scaling relationship between the processed height $\widetilde{h}(t; L)$ and time t for $L = 1024$. A power law was fitted to the data, where the exact relationship was found to be $\widetilde{h}(t; L) = (1.40 \pm 0.01) \cdot t^{(0.54 \pm 0.00)}$.

Overall, when a model obeys the finite-size scaling ansatz (see Equation 6), the data from different system sizes can be collapsed down onto one function, the scaling function (see Equation 5) in our case. Most importantly, the scaling function reveals the common traits amongst different system sizes of the Oslo model, which allows us to predict the statistical behaviour of any given system size with the measurements above.

3.5 Task 2e: Measuring the corrections of scaling

To investigate more carefully the scaling of the average height of the pile, we measured a new set of quantities, including the average height $\langle \widetilde{h}(t; L) \rangle_t$ of the pile, the standard deviation σ_h

of the height and the height probability $P(h; L)$, over one million new grains after the system has reached the steady state.

We can reveal the corrections of scaling for small system sizes by fitting the data with the following equation (see Figure 6):

$$\langle \widetilde{h}(t; L) \rangle_t = a_0 L \left(1 - a_1 L^{-\omega_1}\right), \tag{7}$$

where $\omega_1 > 0$ and a_i are constants. a_0, a_1, ω_1 were measured to be 1.73 ± 0.00, 0.24 ± 0.01 and 0.62 ± 0.02 respectively. From Figure 6, the effect of the corrections is more obvious as the system size decreases, which is evident by the sharp decline for $L < 128$. On the other hand, as L tends to infinity, the correction term decays away and we recover our findings in Section 3.3 where $\langle h(L; t) \rangle \propto L$. This result justifies our decision throughout the project to consider only $L \gg 1$.

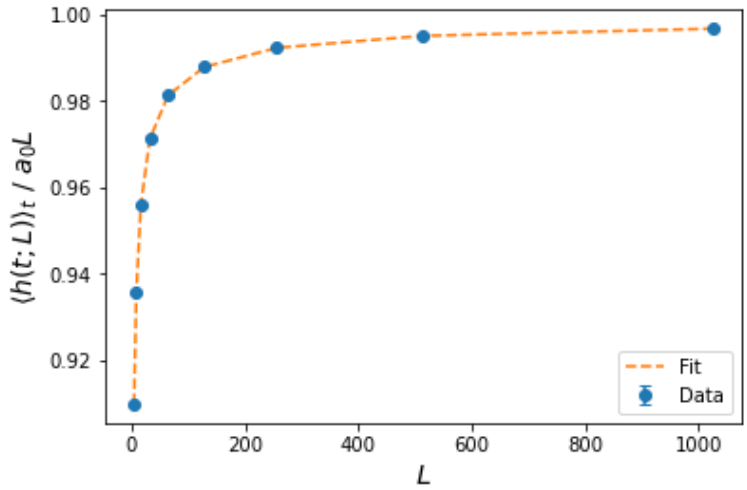

Figure 6: A plot that shows the corrections of scaling for L up to 1024. Equation 7 was fitted to the data, where the exact relationship was found to be $\langle \widetilde{h}(t; L) \rangle_t = (1.73 \pm 0.00) \cdot L \left[1 - (0.24 \pm 0.01) L^{-(0.62 \pm 0.02)}\right]$.

3.6 Task 2f: Measuring the scaling relationship of the standard deviation σ_h of the height

The data for the standard deviation σ_h of the height were fitted with a power law (see Equation 1), the constant of proportionality a was measured to be 0.57 ± 0.00 and the exponent k is 0.24 ± 0.00. This means that as system size increases, there will be a higher number of possible $h(t; L)$.

The knowledge we have had so far allows us to predict the average slope $\langle z(t; L) \rangle$ and its standard deviation σ_z in the limit of $L \to \infty$. Recall from Equation 2 that $h(t; L)$ equals the sum of all the system's local slopes, this is the same as having $h(t; L) = L \cdot \langle z(t; L) \rangle$, thus $\langle z(t; L) \rangle = a_0 = 1.73$ as the correction term vanishes for L approaching infinity. To calculate σ_z, also according to Equation 2, we will have to add the standard deviation of all local slopes in quadrature:

$$\sigma_h^2 = \sum_{i=1}^{L} \sigma_{z_i}^2 = L \cdot \sigma_z^2, \tag{8}$$

assuming that z_i are independent and identically distributed. As a result, we can state that $\sigma_z = \sigma_h / \sqrt{L}$ which becomes 0 as L tends to infinity.

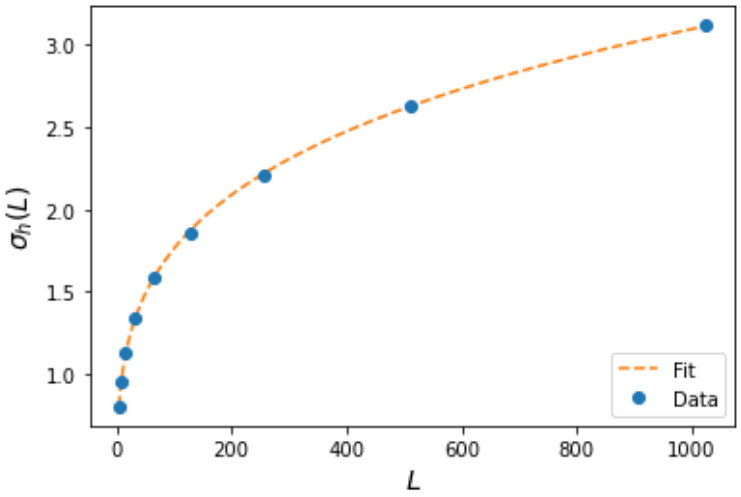

Figure 7: A plot that shows how the standard deviation σ_h of the height scales with the system size L. A power law was fitted to the data, where the exact relationship was found to be $\sigma_h = (0.57 \pm 0.00) \cdot L^{(0.24 \pm 0.00)}$.

3.7 Task 2g: Measuring the height probability $P(h; L)$

3.7.1 i: Theoretical distribution under our assumption

Continuing with our assumption that z_i are independent and identically distributed, we would expect $P(h; L)$ to distribute like a Gaussian as a result of the central limit theorem. This implies that σ_z is a constant independent of system sizes. Thus from Equation 8, we expect σ_h to scale with $\sqrt{L}$.

3.7.2 ii: Producing a data collapse for the height probability $P(h; L)$

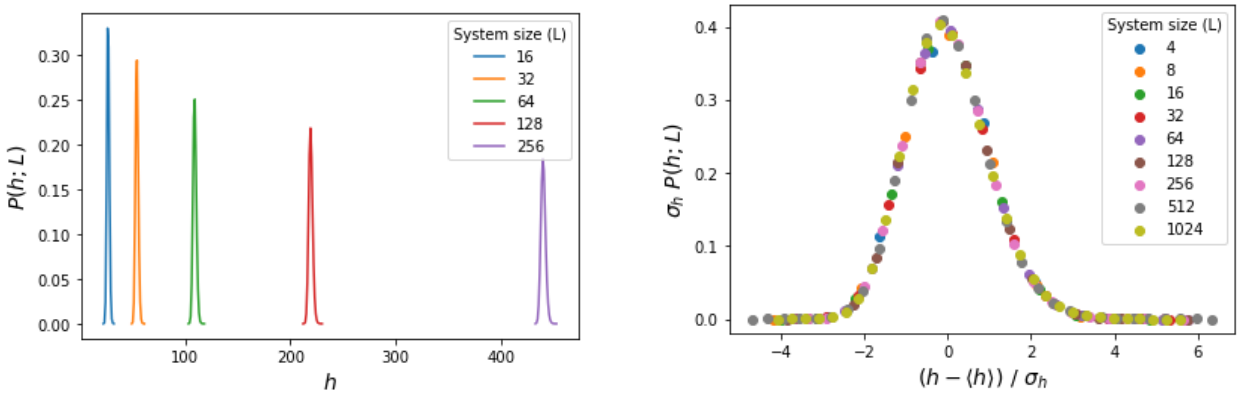

(a) (b)

Figure 8: (a) A plot of the probability distribution $P(h; L)$ against the pile height h for system sizes between 16 and 256. It is evident that σ_h increases for larger system sizes. (b) A data collapse of system sizes up to $L = 1024$. Unlike our prediction, the plot does not resemble a normal distribution owing to its long right tail.

For clarity purposes, we only plotted $P(h; L)$ against $h(t; L)$ for L between 16 and 256. Similar to the previous data collapse, it appears that every system size has its characteristic probability distribution. If in fact $P(h; L)$ for all systems are Gaussian distributed, we would

expect after re-scaling the axes, all data to collapse onto a normal distribution. This involves re-scaling the x-axis to $(h - \langle h \rangle)/\sigma_h$. To ensure that the probabilities sum to unity, we multiplied the y-axis by a normalisation factor which is σ_h in this case. The scaling form is given as follows:

$$P(h; L) = \sigma_h \cdot Z \left(\frac{h - \langle h \rangle}{\sigma_h} \right), \tag{9}$$

where Z is the scaling function.

3.7.3 iii: Explaining the discrepancy in our results

The data collapse from Figure 8b does not agree with our prediction that the scaling function is a normal distribution. The actual function has a long tail on its right-hand side, which indicates that this is instead a skewed Gaussian. Upon examination of the probability distribution for individual system size, it reveals that each function is itself skewed to some degree, meaning that the scaling function does not satisfy the central limit theorem and our assumption stated previously is incorrect. This behaviour was hinted at earlier in Section 3.6 when we fitted σ_h and found that $\sigma_h \propto L^{0.24}$, instead of $\propto L^{0.5}$ as anticipated by the central limit theorem. Intuitively, it is reasonable to think that z_i are not independent because the toppling of one site can affect the slope of another site.

3.7.4 Further measurements

To quantify the distribution of z_i, we measured the average slope $\langle z \rangle$ of $L = 1024$ and obtained a value of 1.73 ± 0.00. This shows that the system tends to preserve $z_i = 2$, reinforcing the argument given in Section 2.3 that $z_i^{th} = 2$ is a less stable state. In addition, using the data for all system sizes, we obtained 0.04 as the skewness for the data collapse.

4 Task 3: Investigating the avalanche-size probability $P(s; L)$ and associated moments s^k

4.1 Task 3a: Producing the data collapse for the avalanche-size probability $P(s; L)$

4.1.1 Method

For the rest of Section 4, we will investigate the normalised avalanche-size probability $\widetilde{P}_N(s; L)$, measured over one million iterations after the system has reached the steady state. As $\widetilde{P}_N(s; L)$ decays according to the power law, we organised our data in exponentially increasing bins (by using the logbin-2020.py file) to ensure that each bin contains roughly the same amount of statistics. This allows a better interpretation of the overall results.

4.1.2 Qualitative explanation of our results

From Figure 9a, we again see that each system is described by its characteristic avalanche-size probability. It is also evident that the number of possible avalanche sizes increases with system size. Every system has an inherent cutoff avalanche size s_c. Before reaching s_c, $\widetilde{P}_N(s; L)$ is described by the power law. Beyond s_c, however, $\widetilde{P}_N(s; L)$ quickly decays away. Given the finite-size scaling ansatz,

$$\widetilde{P}_N(s; L) \propto s^{-\tau_s} \cdot G \left(\frac{s}{L^D} \right), \tag{10}$$

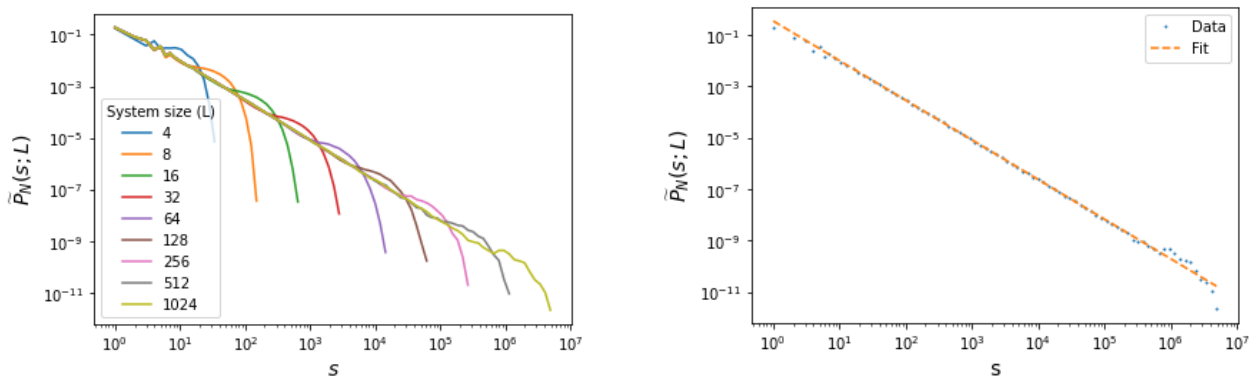

(a) (b)

Figure 9: (a) A plot of the log-binned avalanche-size probability $\widetilde{P}_N(s;L)$ for every system size up to $L = 1024$. The scale parameter was manually adjusted, where we found that having a scale of 1.2 will result in the best statistics for the estimation of the parameters in the data collapse. (b) A plot of the log-binned data for $L = 1024$. A decaying power law was fitted to all data points apart from the first and last 15 to allow estimation for τ_s.

for $L \gg 1$ and $s \gg 1$, we can verify if our data are consistent with a scale-free model by performing a data collapse.

4.1.3 Estimating the values of the avalanche dimension D and the avalanche-size exponent τ_s

To estimate the avalanche-size exponent τ_s, we fitted a decaying power law (see Equation 11) to the log-binned data for $L = 1024$ as it has the largest sample size all system sizes:

$$\widetilde{P}_N(s;L) = a \cdot s^{-\tau_s}. \tag{11}$$

Under pure inspection, it was found that the first and last 15 data points do not obey the power law and were hence discarded from the fit. We measured a to be 0.36 ± 0.00 and also τ_s to be 1.54 ± 0.00. To estimate the avalanche dimension D, we generated a series of data collapse over a range of D values. It was first done with D from 1 to 3 with an increment of 0.2, followed by a more precise trial from 2.10 to 2.30 using a 0.01 step. This then allowed us to inspect by eye and pick the optimal D which gives the best data collapse. This D value was estimated to be 2.15 ± 0.03 where the uncertainty was estimated from the range of indistinguishable frames. Owing to the qualitative nature of this technique, it is difficult to accurately determine τ_s and D.

4.2 Task 3b: Measuring the k'th moment $\langle s^k \rangle$ for k = 1, 2, 3, 4

4.2.1 Measuring the scaling relationship of the k'th moment $\langle s^k \rangle$

The k'th moments $\langle s^k \rangle$ for k = 1, 2, 3, 4 were measured numerically after the system has reached the steady state. Assuming the finite-size scaling ansatz given in Equation 10, we expect:

$$\langle s^k \rangle \propto L^{D(1+k-\tau_s)}, \tag{12}$$

for $L \gg 1$ and $k \geq 1$. This can be proven from first principles considering that $\langle s^k \rangle = \sum_{s=0}^{\infty} s^k \cdot P(s;L)$ [2] but will be stated without proof here. Our data follow a linear relationship with L in a log-log plot which is consistent with the power law scaling anticipated. Taking the logarithm of both sides of Equation 12, we have:

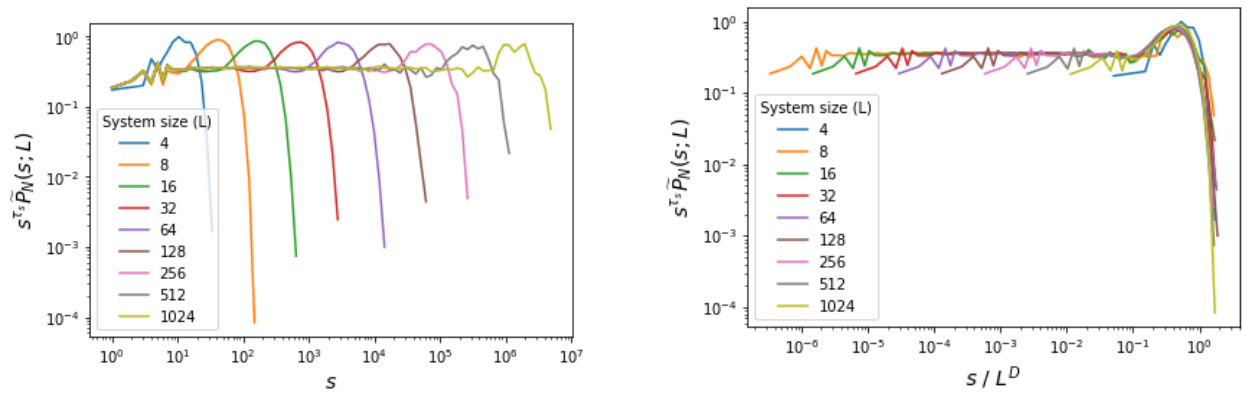

(a) (b)

Figure 10: (a) A plot of the re-scaled probability distribution $s^{\tau_s}P(h;L)$ using the fitted value of τ_s. The distinctive feature of all graphs is aligned vertically (b) A data collapse of system sizes up to $L = 1024$, obtained by systematically changing the D values and selecting the plot of best alignment by eye. Note that to increase the accuracy, we only included $L = 256$, 512 and 1024 during the inspection.

$$\log\langle s^k\rangle = D(1+k-\tau_s)\log L + c, \tag{13}$$

where c is a constant. Thus by fitting each k'th moment in the log-log plot by a linear line (see Figure 11a), we can measure the slope $m = D(1+k-\tau_s)$ for each k. The results of m for $k = 1, 2, 3, 4$ are summarised in Table 1.

4.2.2 Estimating the values of the avalanche dimension D and the avalanche-size exponent τ_s

Finally, plotting each of the slopes against k (see Figure 11b) will allow us to obtain a quantitative estimation of the avalanche dimension D and avalanche-size exponent τ_s.

The gradient of the linear fit in Figure 11b was measured to be 2.23±0.00 and the y-intercept is -1.23 ± 0.01. Judging from the definition of a straight line, we have:

$$y = D(1+k-\tau_s) = m \cdot x + c. \tag{14}$$

Therefore, D equals the gradient and we have $D(1-\tau_s)$ for the y-intercept. We concluded that the values for D and τ_s to be 2.23 ± 0.00 and 1.55 ± 0.00 (Uncertainties were estimated from the covariance matrix). Compared to the textbook values [2], we calculated a -1.33% and a -0.05%, reflecting our results were determined to very high accuracy.

Overall, the moment scaling analysis method provides an alternative way to estimate D and τ_s. Different from the data collapse approach, this method is quantitative in nature and allows more accuracy. In addition with $\langle s^k\rangle = \sum_{s=0}^{\infty} s^k \cdot P(s;L)$, one can predict $P(s;L)$ by simply calculating the k'th moment. This is more convenient as $\langle s^k\rangle$ can be easily determined using a relatively small sample size.

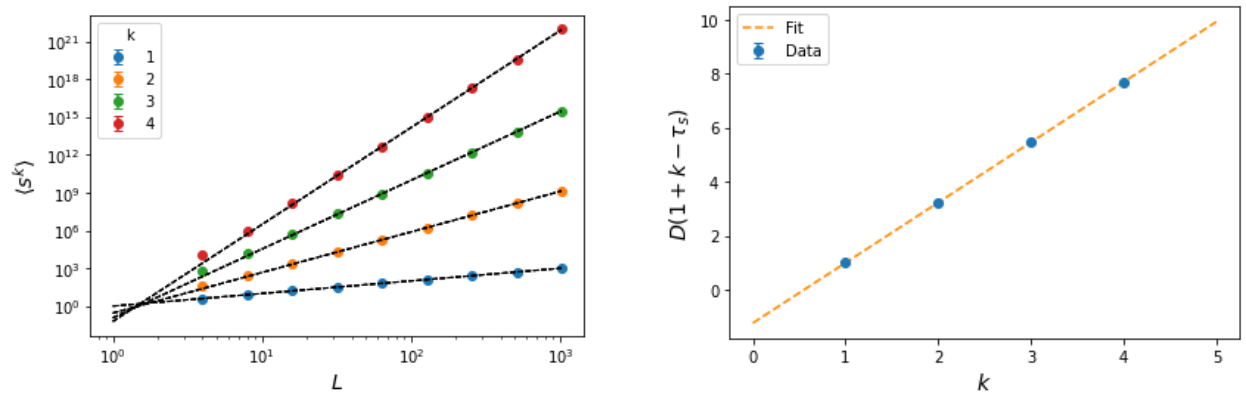

(a) (b)

Figure 11: (a) A plot of the k'th moments $\langle s^k \rangle$ for $k = 1, 2, 3, 4$ in log scales. Linear lines were fitted to $L = 32$ onward only to ensure goodness of fit. (b) A plot of $D(1 + k - \tau_s)$ against k for $k = 1$, 2, 3, 4. Using this plot, D and τ_s were estimated to be 2.23 ± 0.00 and 1.55 ± 0.00.

Table 1: Measurements of $D(1 + k - \tau_s)$ for $k = 1, 2, 3, 4$

k	$D(1 + k - \tau_s)$
1	1.00 ± 0.00
2	3.22 ± 0.00
3	5.45 ± 0.00
4	7.69 ± 0.00

5 Conclusion

The Oslo model displays self-organised criticality, where a system spontaneously drives itself towards a steady state. Notably, at the critical point, the system transitions from the transient configurations to recurrent transitions. At the same time, the model also exhibits a scale-free behaviour for $L \gg 1$, arising from features such as the height of the pile and its avalanche-size probability satisfying the power law. As a result, for any system that obeys the finite-size scaling ansatz, we can collapse our data onto a single function, one which reveals the commonality between all system sizes. Measuring the scaling relationship for a set of quantities thus allows the prediction of the behaviour of any system. The full set of scaling relationships investigated throughout the project are summarised in Table 2.

Table 2: A summary of all scaling relationships measured in this project

Description	Scaling Relationship
Average cross-over time	$\langle t_c(L) = 0.84 \cdot L^{2.00}$
Scaling function for height	$F(x) = 1.40 \cdot x^{0.54}$
Processed height	$\widetilde{h}(t;L) = 1.40 \cdot t^{0.54}$
Corrections of scaling	$\langle \widetilde{h}(t;L) \rangle_t = 1.73 \cdot L\ (1 - 0.24 L^{-0.62})$
Standard deviation of the height	$\sigma_h = 0.57 \cdot L^{0.24}$
Normalised avalanche-size probability	$\widetilde{P}_N(s;L) = 0.36 \cdot s^{-1.54}$
k'th moment	$L^{2.23(1+k-1.55)}$

References

[1] Christensen, K., 2022. Complexity Project Notes. pp.3-7.

[2] Christensen, K. and Moloney, N., 2005. Complexity and criticality. London: Imperial College Press, pp.275, 292, 296.